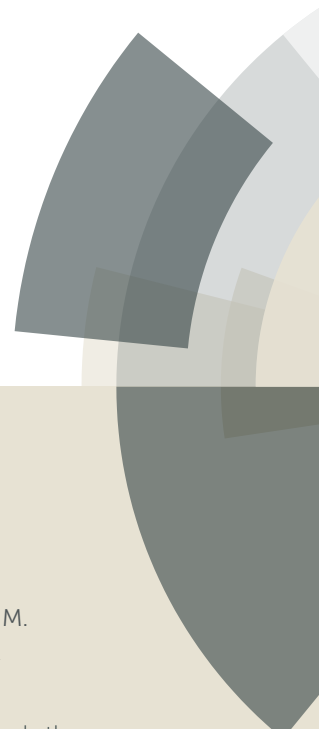


PCCP

Accepted Manuscript



This article can be cited before page numbers have been issued, to do this please use: G. Wiethaus, J. M. Toldo, F. S. Santos, R. D. C. Duarte, P. F.B. Goncalves and F. S. Rodembusch, *Phys. Chem. Chem. Phys.*, 2019, DOI: 10.1039/C8CP05186K.



This is an Accepted Manuscript, which has been through the Royal Society of Chemistry peer review process and has been accepted for publication.

Accepted Manuscripts are published online shortly after acceptance, before technical editing, formatting and proof reading. Using this free service, authors can make their results available to the community, in citable form, before we publish the edited article. We will replace this Accepted Manuscript with the edited and formatted Advance Article as soon as it is available.

You can find more information about Accepted Manuscripts in the [author guidelines](#).

Please note that technical editing may introduce minor changes to the text and/or graphics, which may alter content. The journal's standard [Terms & Conditions](#) and the ethical guidelines, outlined in our [author and reviewer resource centre](#), still apply. In no event shall the Royal Society of Chemistry be held responsible for any errors or omissions in this Accepted Manuscript or any consequences arising from the use of any information it contains.

Experimental and theoretical investigation of long-wavelength fluorescence emission in push-pull benzazoles: intramolecular proton transfer or charge transfer in the excited state?

Guilherme Wiethaus,^a Josene Maria Toldo,^b Fabiano da Silveira Santos,^a Rodrigo da Costa Duarte,^a Paulo Fernando Bruno Gonçalves^{*b} and Fabiano Severo Rodembusch^{*a}

Received 00th January 20xx,
Accepted 00th January 20xx

DOI: 10.1039/x0xx00000x

www.rsc.org/

This study presents the synthesis, characterisation and theoretical calculations of compounds that contain electron donor and withdrawing groups connected through a π -conjugated benzazolic structure. The compounds in solution show an absorption maxima in the UV-visible spectrum (380-390 nm) due to spin and symmetry allowed electronic $^1\pi\pi^*$ with no clear evidence for charge transfer in either compound in the ground state. A fluorescence emission located in the violet-blue-green region, tailored by the solvent polarity, with a large Stokes shift was observed. Taking the long-wavelength emission into account, the Lippert-Mataga plot indicates a positive solvatochromism in the solvent polarity function (Δf) range 0.02-0.20, related to the occurrence of an ICT mechanism in the excited state. At Δf greater than 0.20, the polarity of the medium seems no longer to increase the stabilization of the compounds, reaching a plateau. Time-dependent density functional formalism (TD-DFT) and resolution-identity second-order approximate coupled-cluster (RI-CC2) calculations were also used for better understand the excited state of these compounds. The results indicated that ESIPT is disfavoured in the compounds, mainly in polar solvents, and the emission wavelengths were primarily associated with ICT. In summary, in these push-pull compounds, the electron donating and withdrawing groups do not favour the ESIPT process.

Introduction

Intra or intermolecular proton transfer reactions are one of the most fundamental and important processes in chemistry and biology. Excited state intramolecular proton transfer (ESIPT) was first observed in salicylic acid, as reported by Weller.^{1,2} Since then, a large number of dyes that present ESIPT have been developed and investigated.³⁻⁵ Among them, the benzazoles should be highlighted due to the versatility of the benzazolic ring functionalisation as well as their high thermal and photochemical stability.³ These characteristics, combined with large Stokes shift, allow envisaging several applications for these compounds in the optical sensing and emissive materials domains.⁴⁻¹⁶

Fig. 1 presents the typical ESIPT process for a benzazole dye. The process starts with UV light absorption by the enol-cis conformer (N, left), which in nonpolar or aprotic media is more stable than the enol-open form (N, right).^{17,18} After vertical excitation, the locally excited enol-cis conformer is quickly

converted to the excited keto tautomer (K^*) through an intramolecular proton transfer. The K^* tautomer is usually more stable in the excited state than these locally excited conformers (N^*) and it is the specie responsible for shifting the fluorescence emission band to longer wavelengths. After excited state deactivation, the initial enol form is regenerated without any photochemical change.¹⁸ In many cases, the proton transfer is an ultrafast process that occurs at the sub-picosecond scale¹⁸⁻²⁵ even at low temperatures.⁴

The existence of additional conformers, other than the enol-cis can be directly related to the polarity of the medium. The ESIPT dynamics can compete with solvent polarisation effects. In polar protic solvents, for example, intermolecular hydrogen bonding with the solvent can originate the enol-open conformer (Fig. 1, right) inhibiting ESIPT. Thus, the emission spectra show a band originated from the locally excited conformer (so-called normal emission), at shorter wavelengths, with a small Stokes shift (Fig. 1, top).^{3,26} However, intermolecular hydrogen bonding with the solvent can play a role of a "proton-relay", where the solvent molecules assist ESIPT.^{2,3}

^a Grupo de Pesquisa em Fotoquímica Orgânica Aplicada, Universidade Federal do Rio Grande do Sul - Instituto de Química, Avenida Bento Gonçalves 9500, CEP 91501-970 Porto Alegre-RS, Brazil. Fax: +55 51 33087204; Tel: +55 51 33087206; E-mail: fabiano.rodembusch@ufrgs.br

^b Grupo de Química Teórica e Computacional, Universidade Federal do Rio Grande do Sul - Instituto de Química, Avenida Bento Gonçalves, 9500, CP 15003, CEP 91501-970 Porto Alegre-RS, Brazil; E-mail: paulo@iq.ufrgs.br.

Electronic Supplementary Information (ESI) available: Details for the spectroscopic characterization of the dyes, as well as additional photophysical and computational data can be found in the ESI. See DOI: 10.1039/x0xx00000x

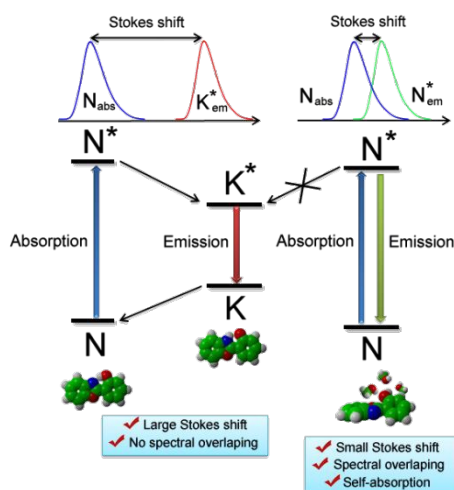


Fig. 1 Förster cycle for the ESIPT process for the 2-(2'-hydroxyphenyl)benzoxazole skeleton. The diagram presents the enol-cis (left), keto tautomer (middle) and enol-open in polar protic solvent (methanol) (right). N and K are related to the normal (enol) and tautomeric (keto) form, respectively. (Adapted from reference 3).

Photoinduced proton transfer can also be affected by the intramolecular charge transfer (ICT). In this case, the competition with the solvent can lead to longer emission wavelengths related to both ESIPT and ICT separately (in a stepwise manner) or coupled (simultaneous manner). The presence of a charge transfer state can be responsible for the strong solvatochromism observed in the fluorescence emission spectra of benzazole dyes.^{27,28} Furthermore, the nature and position of the substituent groups attached to the benzazole core can strongly affect the ICT and ESIPT dynamics, modulating the ESIPT rate ratio.^{29,30} Different substituent groups give rise to different conjugations with the benzazole ring, changing the electronic distribution of the excited state²¹ and, consequently, their spectroscopic properties.^{31,32} Depending on the position of the electron-donor (EDG) or electron-acceptor (EWG) groups attached to the phenyl rings (Fig. 2), a proton transfer can either follow ESIPT or precede it. However, if these events occur at about the same rates, the distinction between both mechanisms is not possible in most of the cases and they are considered as coupled. Several studies deal with the influence of the functional groups attached to the benzazole core in ESIPT.^{23,24,33,34} Generally, benzazole derivatives that contain and EWG at position 6 (see Fig. 2) show ESIPT followed by ICT from the keto tautomer.^{27,30,35,36} On the other hand, in compounds that present an EDG at the same position, ICT occurs prior to ESIPT.^{24,34,37,38} If the position of the substituent group changes, ESIPT and ICT dynamics are affected. For example, changing the $-\text{NH}_2$ substituent from the 6- to the 5-position hastens ICT and disfavours ESIPT due to intermolecular interactions with the solvent.^{2,3}

In compounds that contain an EDG at the 4' position (see Fig. 2), the charge transfer must occur prior to proton transfer, because the acidity of the hydroxyl group is significantly reduced. In this case, ESIPT is still subject to a barrier induced by the solvent polarity, which can control the dynamics of the process. Increasing solvent polarity should stabilise the charge transfer states rather than induce ESIPT process.^{3,30} Thus, the ICT rate is mainly determined by solvent polarity. Therefore, compounds where ESIPT occurs before charge transfer are of great interest, since they must be independent of the relaxation

effects afforded by the solvent. EDGs conjugated with the phenolic hydroxyl group can be strategically inserted into the benzazolic core to allow proton transfer coupled to electron transfer. Although the azolic nitrogen presents a negligible effect on electron transfer, once the proton is transferred, the generated anion becomes a strong EDG that can transfer charge to the EWG via π conjugation.³

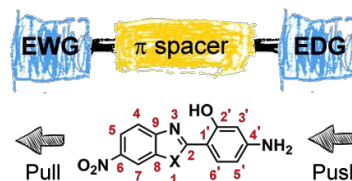


Fig. 2 Chemical structure of the push-pull benzazoles **3a** (X=NH) and **3b** (X=O). Carbon atoms are indicated by red numbers. Abbreviations: EWG, electron-withdrawing group; EDG, electron-donor group.

Based on the interesting photophysical properties of these compounds, this paper reports the synthesis, photophysics and theoretical study of two new benzazole derivatives that simultaneously contain an EDG and EWG at positions 4' and 6, respectively (Fig. 2). In order to better understand the influence of ICT states on ESIPT, time-dependent density functional theory (TD-DFT) was used and two functionals, PBE1PBE³⁹ and CAM-B3LYP,⁴⁰ were evaluated against the resolution-identity second-order approximate coupled-cluster (RI-CC2) method and experimental results. The report on the push-pull effects and the solvent-dependent transition of ICT and the ESIPT emissive states can provide key insights into the intricate environmentally controlled interplay between electronic driving force (ICT) and molecular geometrical stabilities (ESIPT). Our findings could be used to better design new proton-transfer dyes.

Experimental

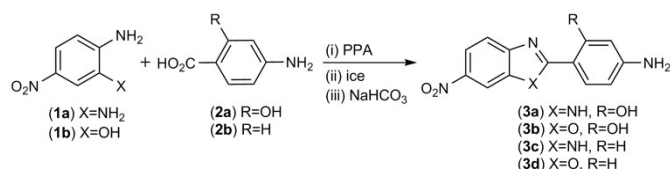
Materials and methods

All reagents and solvents were purchased from commercial suppliers and used without further purification. The solvents were dried and distilled before use based on procedures detailed in the literature.⁴¹ Spectroscopic grade solvents were used for fluorescence and ultraviolet-visible spectrum (UV-Vis) measurements. Elemental analyses were performed with a Perkin-Elmer model 2400. Melting points were measured with a Gehaka PF 1000 apparatus and are uncorrected. Infrared spectra were recorded on a Mattson Galaxy Series FT-IR3000 model 3020 or Varian 640-IR FTIR. ¹H and ¹³C nuclear magnetic resonance (NMR) spectra were performed on a VARIAN INOVA YH300 using tetramethylsilane (TMS) as the internal standard and dimethyl sulfoxide ($\text{DMSO}-d_6$) (Sigma-Aldrich) as the solvent at room temperature. The chemical shifts (δ) are reported in parts per million (ppm) relative to TMS (0.00 ppm), and the coupling constants (J) are reported in hertz (Hz). High resolution mass spectrometry was recorded with electrospray ionization (HRMS-ESI) data in the positive mode using a Q-TOF-MS Bruker Impact II. UV-Vis absorption spectra were obtained with a Shimadzu UV-2450 spectrophotometer. Steady state fluorescence spectra were measured with a Shimadzu

spectrofluorometer (model RF-5301PC). All experiments were performed at room temperature (25°C). The quantum yield of fluorescence (QY) was measured at 25°C using spectroscopic grade solvents within solutions with absorbance intensity lower than 0.05 (optical dilute methodology). Quinine sulfate (Riedel) in 1 N H₂SO₄ was used as the QY standard.⁴²

Synthesis

The ES IPT (**3a-b**) and non-ES IPT (**3c-d**) benzazoles were synthesised from an adapted synthetic methodology previously described in the literature (Scheme 1).^{32,43}



Scheme 1 Synthetic route for obtaining benzazoles **3a-d**.

The benzazole derivatives (**3a-d**) were synthesised by reaction of 1.0 g (6.59 mmol) of the respective nitroaniline (**1a-b**) with 1.0 g (6.59 mmol) of 4-aminosalicylic acid (**2a**) or 1.0 g (7.29 mmol) of 4-aminobenzoic acid (**2b**) in 20 ml of polyphosphoric acid (PPA). To better solubilise the reagents into the solvent, the PPA was previously heated to 60°C under vigorous stirring. Then, the reaction mixture was heated under an N₂ atmosphere at 60°C for 1 h, 120°C for 2 h and, finally, 180°C for more 2 h. The reaction mixture was poured into crushed ice, with stirring, and neutralised with NaHCO₃ (10%). The dark precipitate obtained was filtered, washed with water (3 x 20 mL) and dried at room temperature. A previous purification was performed using a Soxhlet extractor with acetone as the solvent. The solvent was removed under reduced pressure, and the obtained solid was purified by column chromatography on silica gel 60 (0.063-0.200 mm) using CH₂Cl₂/acetone (92:8) (for **3a**), acetone (for **3b**), CHCl₃/acetone (10:1) (for **3c**) and CHCl₃/acetone (20:1) (for **3d**) as the eluents.

2-(4'-Amino-2'-hydroxyphenyl)-6-nitrobenzimidazole (3a). Pale orange solid. Yield: 28%. ¹H NMR (300 MHz, DMSO-*d*₆, δ ppm) 13.07 (broad s, 1H, OH); 12.27 (broad s, 1H, NH); 8.35 (s, 1H, H7); 8.08 (dd, 1H, H5, *J*_m=1.8 Hz, *J*_o=8.7 Hz); 7.72 (d, 1H, H6', *J*_o=8.7 Hz); 7.65 (d, 1H, H4, *J*_o=8.7 Hz); 6.25 (d, 1H, H5', *J*_m=1.5 Hz, *J*_o=8.4 Hz); 6.17 (d, 1H, H3', *J*_m=1.5 Hz); 5.99 (s, 2H, NH₂). ¹³C NMR (75 MHz, DMSO-*d*₆, δ ppm) 160.4, 154.0, 128.7, 118.3, 107.1, 100.8, 100.2. FTIR (KBr, ν=cm⁻¹) 3481, 3393, 3273, 3242, 1650, 1422, 1520, 1334. Anal. calcd. for C₁₃H₁₀N₄O₃ (270.24 g·mol⁻¹): C 57.78; H 3.73; N 20.73. Found: C 58.21; H 3.73; N 20.01. HRMS-ESI [M+H]⁺ calcd for [C₁₃H₁₁N₄O₃]⁺: 271.0831, found 271.0826.

2-(4'-Amino-2'-hydroxyphenyl)-6-nitrobenzoxazole (3b). Orange solid. Yield: 36%. ¹H NMR (300 MHz, DMSO-*d*₆, δ ppm) 10.89 (s, 1H, OH); 8.59 (d, 1H, H7, *J*_m=1.8 Hz); 8.27 (dd, 1H, H5, *J*_m=2.1 Hz, *J*_o=8.4 Hz); 7.83 (d, 1H, H4, *J*_o=8.7 Hz); 7.68 (d, 1H, H6', *J*_o=8.7 Hz); 6.38 (s, 2H, NH₂); 6.32 (d, 1H, H5', *J*_m=2.1 Hz,

*J*_o=8.7 Hz); 6.18 (d, 1H, H3', *J*_m=2.1 Hz). ¹³C NMR (75 MHz, DMSO-*d*₆, δ ppm) 168.1, 160.9, 156.3, 148.2, 146.5, 143.9, 129.7, 121.6, 117.9, 108.2, 107.0, 99.0, 97.4. FTIR (KBr, ν=cm⁻¹) 3481, 3383, 3233, 1636, 1439, 3123, 1502. Anal. calcd. for C₁₃H₉N₃O₄ (271.23 g·mol⁻¹): C 57.57; H 3.34; N 15.49. Found: C 57.72; H 3.49; N 14.62. HRMS-ESI [M+H]⁺ calcd for [C₁₃H₁₀N₃O₄]⁺: 272.0671, found 272.0666.

2-(4'-Aminophenyl)-6-nitrobenzimidazol (3c). Yield: 10%. FTIR (KBr, ν=cm⁻¹) 3481, 3383, 3233, 1636, 1439, 3123, 1502 and 1323. ¹H NMR (300 MHz, DMSO-*d*₆, δ ppm) 10.89 (s, 1H, OH); 8.59 (d, 1H, H7, *J*_m=1.8 Hz); 8.27 (dd, 1H, H5, *J*_m=2.1 Hz, *J*_o=8.4 Hz); 7.83 (d, 1H, H4, *J*_o=8.7 Hz); 7.68 (d, 1H, H6', *J*_o=8.7 Hz); 6.38 (s, 2H, NH₂); 6.32 (d, 1H, H5', *J*_m=2.1 Hz, *J*_o=8.7 Hz); 6.18 (d, 1H, H3', *J*_m=2.1 Hz). Anal. calcd. for C₁₃H₁₀N₄O₂ (254.24 g·mol⁻¹): C 61.41; H 3.96; N 22.04. Found: C 60.89; H 3.77; N 21.70. HRMS-ESI [M+H]⁺ calcd for [C₁₃H₁₁N₄O₂]⁺: 255.0882, found 255.0877.

2-(4'-Aminophenyl)-6-nitrobenzoxazol (3d). Yield: 8%. FTIR (KBr, ν=cm⁻¹) 3468, 3358, 3328, 1640, 1436, 3115, 1515 and 1339. ¹H NMR (300 MHz, DMSO-*d*₆, δ ppm) 8.54 (d, 1H, H7, *J*_m=2.1 Hz); 8.24 (dd, 1H, H5, *J*_m=2.1 Hz and *J*_o=8.7 Hz); 7.90 (dd, 2H, H2' and H6', *J*_o=8.7 Hz); 7.80 (d, 1H, H4, *J*_o=8.7 Hz); 6.72 (dd, 2H, H3' and H5', *J*_o=8.7 Hz); 6.29 (s, 2H, NH₂). Anal. calcd. for C₁₃H₉N₃O₃ (255.23 g·mol⁻¹): C 61.18; H 3.55; N 16.46. Found: C 60.66; H 3.02; N 15.88. HRMS-ESI [M+H]⁺ calcd for [C₁₃H₁₀N₃O₃]⁺: 256.0722, found 256.0717.

Theoretical calculations

Theoretical studies of ES IPT in large systems are computationally expensive to employ high-level ab initio calculations. Thus, due to its cost-benefit, many publications adopt time-dependent density functional theory (TD-DFT).^{8,24,36-38,44-46} Additionally, studies using RI-CC2,^{19,22,47,48} multireference methods⁴⁹⁻⁵² and semi-classical dynamics are also reported.^{18,22,48,53} The ground electronic state and first excited state equilibrium geometries were obtained by optimising the geometries using PBE1PBE and CAM-B3LYP functionals together with cc-pVDZ basis set. Subsequently, single-point TD-DFT calculations were performed using both functionals but larger basis set (jun-cc-pVTZ) in order to obtain the vertical absorption, vertical emission, and population analysis.¹⁴ The jun- type basis set, named calendar basis set, is recommended by Truhlar *et al.* as a good alternative to the highly costly augmented (aug) basis sets because of its performance versus cost.⁵⁴ The calendar basis set is constructed by removing diffuse functions from the aug basis sets. All equilibrium geometries were confirmed by vibrational analysis, having no imaginary frequencies. Solvent effects were included in all cases by the integral equations formalism of the polarisable continuum model (IEF-PCM).¹⁵ The solvents considered were 1,4-dioxane, dichloromethane, ethanol and acetonitrile. The electrostatic potential surfaces in the ground and excited states, atomic charges, and dipole moment were obtained by population analysis using Charges from Electrostatic Potential using a Grid-based method (ChelpG).²⁰ Relaxed scans for the proton transfer coordinate between enol and keto tautomers were done at the first excited state potential energy surface for **3a** and **3b**. To further evaluate the

proton transfer in these compounds, relaxed scans for 2-2'-hydroxyphenylbenzoxazole (HBO) in the S_1 state were also performed. For these calculations, the geometries were optimised by increasing the O–H bond distance by 0.05 Å for each step using the CAM-B3LYP/cc-pVDZ level of theory and IEF-PCM/1,4-dioxane as the implicit solvent. The calculations were carried out using Gaussian 09 Revision D.01. RI-CC2 is suitable to provide benchmark results for TD-DFT calculations^{55,56} and was used for comparison with the results obtained by using PBE1PBE and CAM-B3LYP functionals. RI-CC2 single point calculations in the gas phase at the optimised TD-DFT geometries were performed by employing the aug-cc-pVDZ basis using Turbomole 7.0 package.⁵⁷

Results and discussion

UV-Vis absorption

The normalised absorption spectra of benzazoles **3a** and **3b** are shown in Fig. 3, and the relevant data calculated from UV-Vis absorption spectroscopy are presented in Table 1.

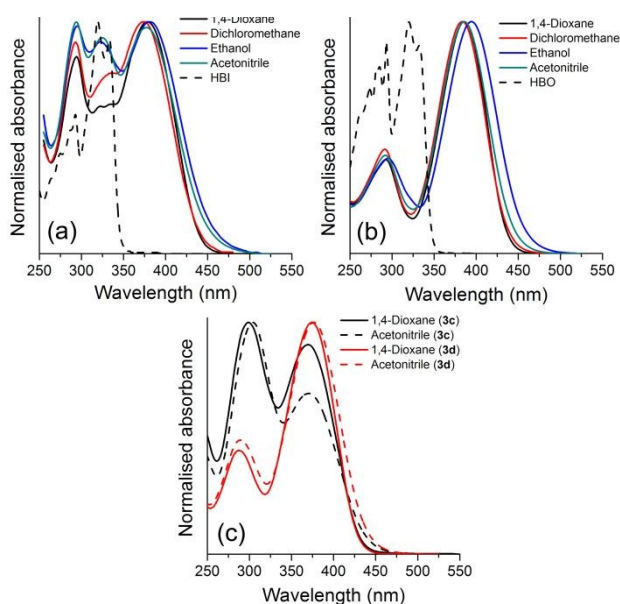


Fig. 3 Normalised UV-Vis absorption spectra in solution for benzazoles (a) **3a**, (b) **3b** and (c) non-ESIPT benzazoles **3c-d** at 10^{-5} M. For comparison, the respective benzazoles without the EWG and EDG groups, 2-2'-hydroxyphenyl)benzimidazole, (HBI) and 2-2'-hydroxyphenylbenzoxazole (HBO), are also presented in dichloromethane.

The push-pull benzazole **3a** presented absorption maxima located around 375 nm. A small solvatochromic effect ($\Delta\lambda_{\text{abs}}$ 7 nm) was observed, indicating an almost absent of charge transfer character in the ground state. Compound **3b** presented absorption maxima located around 385 nm and a slightly higher solvatochromic effect ($\Delta\lambda_{\text{abs}}$ 11 nm). In all the solvents, the oxygenated derivative **3b** presented a red shifted absorption compared to the nitrogenated analogue **3a**. The observed redshift values for the absorption maxima in ethanol are probably due to specific solvent-solute interaction, such as

Table 1 Relevant photophysical data of the UV-Vis absorption spectra, where λ_{abs} is the absorption maxima (nm), ϵ is the molar absorptivity coefficient ($10^4 \text{ M}^{-1}\text{cm}^{-1}$), f_e is the calculated oscillator strength, k_e^0 is the calculated radiative rate constant (10^8 s^{-1}) and τ^0 is the calculated pure radiative lifetime (in ns).

Benzazole	Solvent	λ_{abs}	ϵ	f_e	k_e^0	τ^0
3a	1,4-Dioxane	378	2.17	0.46	3.21	3.11
	Dichloromethane	373	1.18	0.20	1.47	6.82
	Ethanol	380	1.68	0.34	2.36	4.24
	Acetonitrile	377	1.70	0.34	2.43	4.12
3b	1,4-Dioxane	386	3.36	0.63	4.25	2.35
	Dichloromethane	383	5.26	0.91	6.20	1.61
	Ethanol	394	3.61	0.74	4.74	2.11
	Acetonitrile	386	2.15	0.42	2.81	3.56
3c	1,4-Dioxane	370	1.88	0.32	2.31	4.33
	Acetonitrile	370	1.71	0.34	2.46	4.07
3d	1,4-Dioxane	374	2.63	0.48	3.46	2.89
	Acetonitrile	376	3.00	0.61	4.34	2.31

hydrogen bonding.⁵⁸ When compared to their analogues benzazolic molecules without the EWG (nitro) and EDG (amino) groups, the so-called HBI and HBO, both compounds present redshifted bands (around 60 nm) in dichloromethane, as expected.⁵⁹ The simultaneous presence of the amino group in the 4' position and the nitro group at the 6 position lead to the extension of the chromophore through the benzazolic core and, consequently, to a pronounced bathochromic shift in the absorption spectra. It is worth mentioning that the chromophore extension is not possible when the EWG and EDG groups are attached at different positions.³⁰

In order to better understand the photophysical behavior in the ground state of the studied compounds **3a** and **3b**, the non-ESIPT benzazoles (**3c** and **3d**) were also evaluated via UV-Vis absorption spectroscopy in solution using 1,4-dioxane and acetonitrile as solvents (Fig. 3 and Table 1). These compounds present similar chemical structures to **3a** and **3b** but without the hydroxyl group at position 2' and show absorption maxima located around 370 nm and 375 nm, respectively with absent solvatochromic effect, indicating that the auxochrome group hydroxyl plays an important role on the π conjugation of these compounds, as expected.

From the UV-Vis absorption spectra, oscillator strengths (f_e), radiative rate constants for emission (k_e^0), which is the probability of emission of photons per time unit, as well as pure radiative lifetimes (τ^0) were calculated. The first one, f_e , was calculated by applying the Strickler-Berg equation (Equation 1).⁶⁰

$$f_e = 4.32 \times 10^{-9} \int \epsilon(\bar{\nu}) d\bar{\nu}, \quad (1)$$

where the integral is the area under the absorption spectra curves from plotting the molar absorptivity coefficient ϵ ($\text{M}^{-1}\text{cm}^{-1}$) against wavenumber $\bar{\nu}$ in (cm^{-1}). k_e^0 can be obtained in a similar way, using Equation (2).

$$k_e^0 \approx 2.88 \times 10^9 \bar{\nu}_0^2 \int \epsilon(\bar{\nu}) d\bar{\nu}, \quad (2)$$

where $\bar{\nu}_0$ is the wavenumber corresponding to the maximum absorption wavelength. The pure radiative lifetime, τ^0 , is defined as $1/k_e^0$.⁶¹

The high values obtained for ϵ ($\sim 10^4 \text{ M}^{-1}\text{cm}^{-1}$, Table 1), as well as the calculated radiative rate constant (k_e^0) can be related

to $^1\pi\pi^*$ transitions for the studied benzazoles **3a-d**. The f_e values obtained from the experiments also corroborate with $^1\pi\pi^*$ electronic dipole-allowed transitions since they are comparable to the expected ones for the $^1\pi\pi^*$ transitions ($f_e \approx 10^{-3}-1$).⁶² The calculated τ^0 values indicate that after absorption of radiation, these benzazoles populate the same excited state.

Fluorescence emission

The normalised fluorescence emission spectra of compounds **3a** and **3b** are presented in Fig. 4. The emission curves were obtained by exciting the compounds at the respective absorption maxima wavelength. The relevant data from the fluorescence emission spectroscopy are summarised in Table 2.

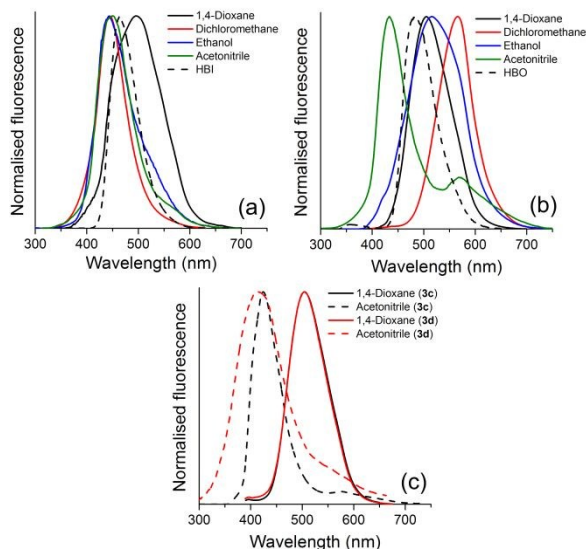


Fig. 4 Normalised emission spectra in solution for benzazoles (a) **3a**, (b) **3b** and (c) non-ESIPT benzazoles **3c-d** at 10^{-5} M. For comparison, the respective benzazoles without the EWG and EDG groups, 2-2'-hydroxyphenylbenzimidazole, (HBI) and 2-2'-hydroxyphenylbenzoxazole (HBO), are also presented in dichloromethane.

Benzazole **3a** presented emission maxima located in the blue-green region (441-497 nm). However, unexpectedly, a redshift higher than 50 nm was observed using 1,4-dioxane. In this solvent, considering the full width at the half maximum (FWHM) of the emission band (FWHM=119.0 in 1,4-dioxane and 62.6 in dichloromethane) and the location of the observed shoulder (~ 450 nm), we could assign the emission peak to: (i) both locally excited (LE) and ICT contributions or (ii) locally excited (LE) and ICT coupled to ESIPT process. In both propositions, the locally excited (LE) emission band can be related to the observed shoulder around 450 nm, since there is no influence of the solvent polarity on this location (see Fig. S12). The emission maximum can be related to an ICT character, observed by the redshift from 500 nm up to 550 nm (see Fig. S12) increasing the medium polarity. However, the second explanation, ICT coupled to ESIPT process, cannot be discarded since the main emission band, despite the observed redshift, presents a decrease on its intensity increasing the

Table 2 Relevant photophysical data of the fluorescence emission spectra, where λ_{em} is the emission maxima (nm), $\Delta\lambda_{ST}$ is the Stokes shift (nm) and Φ_F is the fluorescence QY.

Benzazole	Solvent	λ_{em}	$\Delta\lambda_{ST}$	Φ_F
3a	1,4-Dioxane	497	6335	0.009
	Dichloromethane	444	4288	0.007
	Ethanol	443	3742	0.008
	Acetonitrile	449/563	4254/8764	0.005
3b	1,4-Dioxane	505	6105	0.100
	Dichloromethane	564	8343	0.018
	Ethanol	516	6001	0.073
	Acetonitrile	434/571	2865/8393	0.010
3c	1,4-Dioxane	505	7226	0.027
	Acetonitrile	424/576	3443/9666	0.001
3d	1,4-Dioxane	504	6896	0.059
	Acetonitrile	414/556	2441/8610	0.001

medium polarity. It is worth mentioning that the parent compound **3c** show a quite similar photophysics in 1,4-dioxane, with a main emission band located above 500 nm, but a FWHM below 90 nm (Fig. 4). Since, this compound is not able to ESIPT due to the absence of the hydroxyl moiety, and the half maximum (FWHM) of the emission band is significantly smaller than those observed for **3a** in the same solvent, it is believed that the second proposition, ICT coupled to ESIPT process, are probably taking place in the excited state for this compound in such solvent.

It is therefore difficult to assign from the experimental results, the emitting species definitively in this case, as already observed for different proton-transfer compounds.⁶³ Although HBO presented emission maxima in the same range of **3a** (Fig. 4 top, dashed line) it is worth mentioning that different photophysical behaviour takes place for these two compounds. It is well known that HBO presents ESIPT, and therefore its emission is attributed to the keto tautomer, with a Stokes shift greater than 9000 cm^{-1} .⁵

Compound **3b** presented emission maxima above 500 nm, redshifted compared to **3a**. Despite the emission value in ethanol, which was strongly affected by the solvent-fluorophore hydrogen bonding, **3b** presents a redshift on the maxima location for the long-wavelength emission as solvent polarity increased. In 1,4-dioxane, due to the maxima location and Stokes shift value, it seems that the same explanation proposed to **3a** can be used for this compound. In acetonitrile, compound **3a** presented dual fluorescence emission. A main emission band located at 449 nm and a less intense redshifted band located at 563 nm, a quite similar behaviour to that observed for the non-ESIPT analogue **3d** (Fig. 4). In this way, it is believed that the dual fluorescence emission can be related to locally excited (short wavelength) and ICT (long wavelength) character. Compound **3b** also presents in acetonitrile a dual fluorescence emission with maxima located at 434 nm and 571 nm. The character of the long-wavelength was properly answered also regarding the **3d**, that is not able to ESIPT, where dual fluorescence emission was clearly observed located at 414 nm and 556 nm. This result strongly indicates that in this solvent, **3b** also presents a locally excited (LE) and ICT contributions.

Lippert-Mataga correlation and NLO properties

In order to better correlate the observed differences on the calculated Stokes shift with ICT or ESPT in **3a** and **3b**, the solvent polarity plot function was obtained (Fig. 5).⁶⁴ Here, the differences in the dipole moment between the excited and ground states were calculated by applying the Lippert-Mataga relation (Equation 3):⁶⁴

$$\Delta\bar{\nu}_{st} = \frac{2\Delta\mu_{eg}^2}{hca^3}\Delta f + constant \quad (3)$$

In this equation, h is the Planck's constant, c is the speed of light, a is the Onsager cavity radius and $\Delta\mu_{eg}^2$ is the difference in the dipole moment between the excited and ground states for the studied compounds. In the Lippert-Mataga relation, the solvent polarity function (Δf) can be obtained from Equation (4),^{58,60}

$$\Delta f = \frac{(\varepsilon - 1)}{(2\varepsilon + 1)} - \frac{(n^2 - 1)}{(2n^2 + 1)} \quad (4)$$

where the dielectric constant (ε) and the refractive index (n) for a mixture of solvents can be calculated by the following equations:⁵⁸

$$\varepsilon_{mix} = f_A \cdot \varepsilon_A + f_B \cdot \varepsilon_B \quad (5)$$

$$n_{mix}^2 = f_A n_A^2 + f_B n_B^2 \quad (6)$$

In Equations (5) and (6), f_A and f_B are the volumetric fractions of the two solvents. A linear plot of the absorbance, fluorescence emission or Stokes shift versus the solvent polarity function indicates the internal charge transfer character.⁶⁵ By applying the Lippert-Mataga correlation, there was no clear evidence for charge transfer in either compound in the ground state (Fig. 5a). The original spectra can be seen in Fig. S11.

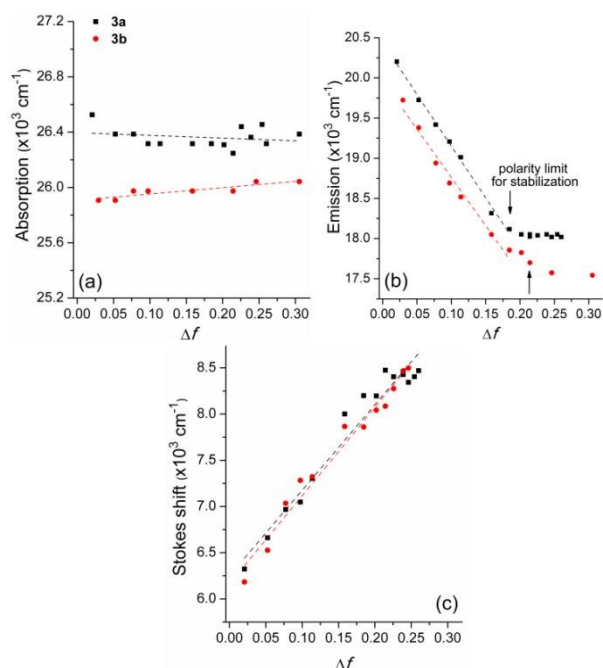


Fig. 5 Solvent effects on the spectral position of **3a** and **3b** taking the (a) absorption, (b) emission and (c) Stokes shift into account.

Even though the variation is small, compound **3b** was more destabilised in more polar environments than the nitrogen

analogue (**3a**). On the other hand, in the excited state, and taking the longer emission wavelengths above 500 nm into account (see Fig. S12), it was observed a positive solvatochromism. The fluorescence maxima against Δf in the 0.02–0.20 range presented a linear correlation ($R^2=0.99$ and 0.98 for **3a** and **3b**, respectively), a finding which corroborates the occurrence of an ICT mechanism in the excited state, as already observed for similar structures.^{2,24,27,36} Additionally, in more polar media, with an solvent polarity function greater than 0.20, the emission maxima location no longer redshifted but maintained the large Stokes shift. A possible explanation could be that the polarity medium seems no longer to increase the stabilization of the compounds, reaching a limit.

Nonlinear optics (NLO) is concerned with how the electromagnetic field of a light wave interacts with the electromagnetic fields of matter and other light waves.⁶⁶ Sohn *et al.* affirms that the interaction of light with a NLO material will causes changes in its properties where the next photon will experience a structure with different properties. In these materials, strong interactions can disturb the frequency, phase, polarisation, or path of the incident light. In this sense, it is worth investigating the NLO properties of **3a** and **3b** in order to understand how matter, and specifically the electronic charge density in matter, interacts with light.⁶⁶ It was obtained NLO properties by applying the solvatochromic method,^{67,68} compounds **3a** and **3b** presented high first hyperpolarisabilities (β) achieved by Hyper-Rayleigh Scattering.^{32,43} In this methodology, the first polarisability (α_{xx}) and first order hyperpolarisability (β_{xxx}) were determined from the ground state data, as summarised in Tables 3 and 4. The linear polarisability α_{xx} (in cm^3) was calculated according to Equation (7):⁶⁹

$$\alpha_{xx} = 2 \frac{\mu_{ge}^2}{E_{ge}}, \quad (7)$$

where E_{ge} is the energy difference from the ground to excited state charge transfer transition, in erg .⁷⁰⁻⁷² In this equation, μ_{ge} is the experimental transition dipole moment given by Equation (8), where f is the oscillator strength and $\bar{\nu}$ is absorption wavenumber, in cm^{-1} .⁶⁹

$$\mu_{ge} = \sqrt{\frac{f}{4.7016 \times 10^{-7} \bar{\nu}}} \quad (8)$$

Compound **3a** presented higher values to the experimental transition dipole moment (μ_{ge}) if compared to the analogue **3b** (Table 3). Further, both compounds showed similar values for the energies of ground to excited state charge transfer transition (E_{ge}). The linear polarisability α_{xx} values ranged from 0.61×10^{-23} to $2.89 \times 10^{-23} \text{ cm}^3$. Compound **3a** presented lower α_{xx} values compared to **3b**, as already observed for the benzimidazole derivative when compared to benzoxazole one.^{32,43} In this sense, it is believed that in the presence of an external electromagnetic field, **3b** will produce a more intense displacement of the electron density away from the nucleus, a phenomenon that would result in a charge separation (induced dipole).⁶⁶

Table 3 Table of constants, where μ_{ge} is the experimental transition dipole moment (in Debye), E_{ge} is the energy of ground to excited state charge transfer transition (10^{-12} erg) and α_{xx} is the linear polarizability (10^{-23} cm³).

Benzazole	Solvent	μ_{ge}	E_{ge}	α_{xx}
3a	1,4-Dioxane	6.08	5.26	1.41
	Dichloromethane	4.02	5.33	0.61
	Ethanol	5.25	5.23	1.05
	Acetonitrile	5.26	5.27	1.05
3b	1,4-Dioxane	7.21	5.15	2.02
	Dichloromethane	8.64	5.17	2.89
	Ethanol	7.86	5.04	2.45
	Acetonitrile	5.86	5.15	1.34

It was applied Equation (9) in order to compute first order hyperpolarisability (β_{xxx}).⁷² The obtained values are summarised in Table 4.

$$\beta_{xxx} = 6 \frac{\mu_{ge}^2}{E_{ge}^2} \Delta\mu_{eg}, \quad (9)$$

where μ_{ge} is the transition dipole moment (in esu-cm), E_{ge} is the energy of the transition from the ground to the excited state charge transfer (in erg), and $\Delta\mu_{eg}$ is the difference between the excited and ground state dipole moments (in esu-cm).⁷² This last parameter can be obtained from the McRae polarity function (Equation 10):⁷²⁻⁷⁴

$$\bar{\nu}_{abs} - \bar{\nu}_{em} = \frac{2\Delta\mu_{eg}^2}{hca^3} \left(\frac{\epsilon - 1}{\epsilon + 2} - \frac{n^2 - 1}{n^2 + 2} \right) + (\delta_{abs} + \delta_{em}). \quad (10)$$

In this equation $\bar{\nu}_{abs} - \bar{\nu}_{em}$ is the Stokes shift (in cm⁻¹), δ_{abs} and δ_{em} are the differences in the vibrational energy (in cm⁻¹) of the molecule in the ground and excited states for absorption and emission, respectively, h is the Planck's constant (in erg-s), c is the speed of light in a vacuum (in cm-s⁻¹), ϵ is the relative dielectric constant and n is the static refractive index of the solvent. Thus, Equation (10) can be rewritten as Equation (11):

$$y = mx + c \quad (11)$$

where:

$$y = \bar{\nu}_{abs} - \bar{\nu}_{ems}$$

$$x = \left(\frac{\epsilon - 1}{\epsilon + 2} - \frac{n^2 - 1}{n^2 + 2} \right)$$

$$m = \frac{2\Delta\mu_{eg}^2}{hca^3} \text{ and}$$

$$c = \delta_{abs} + \delta_{em}.$$

In this study, it was obtained the Onsager cavity radius (a) in the gas phase using the CAM-B3LYP/jun-cc-pVTZ theory level. In Equation (11), it was used Onsager radii 0.5 Å smaller than those calculated, as recommended in the literature⁷⁵ (5.01 and 4.99 Å for **3a** and **3b**, respectively). The differences between the ground state and excited state dipole moments ($\Delta\mu_{eg}$) in different solvents were calculated using the slope and Onsager radii of the molecules in their solvent environments. Once again, compound **3b** presented higher values (2.15 D) for $\Delta\mu_{eg}$ compared to the benzimidazole derivative **3a** (1.98 D). Moreover, the values for first hyperpolarisability obtained using the solvatochromic method indicated that **3a** and **3b** present values of β_{xxx} 32 to 83 times greater than urea.

Table 4 Table of constants, where a is the cavity radius within Onsager's model (in 10^{-8} cm), $\Delta\mu_{eg}$ is the difference between the ground state and excited state dipole moments (in Debye) and β_{xxx} is the first hyperpolarisability (in 10^{-30} cm⁵·esu⁻¹).

Benzazole	a^a	$\Delta\mu_{eg}$	β_{xxx}	$x\beta_{urea}^b$
3a	4.51	1.98	12.0	32
3b	4.49	2.15	31.4	83

^aOnsager cavity radius was obtained in the gas phase using CAM-B3LYP/jun-cc-pVTZ level of theory. ^bUrea: $\beta_{xxx} = 0.38 \times 10^{-30}$ cm⁵·esu⁻¹.⁷²

Usually, the first hyperpolarisability mainly depends on conjugation path length and strength of electron donor and electron acceptor group.⁷¹ In this way, although **3a** and **3b** have a strong EDG (NO₂), the obtained values for β_{xxx} compared with the ones obtained for urea are probably tailored not only by molecular conjugation of the benzazolic ring but also by the relatively weak EDG (NH₂).

Theoretical calculations

The keto and enol conformers were optimized in the ground and first excited state using DFT and TD-DFT, respectively. Two different exchange-correlation functionals were used, the hybrid PBE1PBE, which is reported to give good results for benzazole derivatives,⁷⁶⁻⁷⁸ and CAM-B3LYP, which includes long-range corrections, in order to deal with excited states which present an ICT character.²³

All the conformers found for **3a** and **3b** in the ground state are presented in Figs. S14 and S15, respectively. The correspondent energies are summarised in Tables S1 and S2. Similar to the non-substituted benzazoles HBO and HBI,⁷⁹ in the gas phase or in low polarity solvents the most stable conformation in the ground state was the so-called enol-cis (E_{cis} ; Fig. 6).

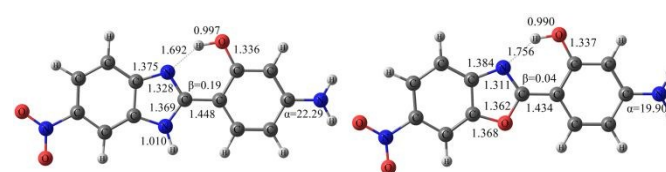


Fig. 6 Most stable structures for **3a** (left) and **3b** (right) in the ground state, using CAM-B3LYP/cc-pVDZ and PCM/1,4-dioxane. The bond lengths are presented in Ångstroms and the dihedral angles in degrees.

In this conformation, benzazole and phenyl rings are in the same plane and there is a hydrogen bonding between O—H...N atoms. In the ground state, the keto tautomers were broadly disfavoured by, at least, 10 kcal·mol⁻¹. They could be obtained only by imposing constraints in geometry optimisation. The main change in the geometries of the ground states was observed in the NH₂ group. While E_{cis} presents a planar structure, with the hydrogens in the same plane of the phenol ring, the remaining structures have a pyramidalised NH₂, with out-of-the-plane hydrogens (Figs. S13 and S14). Another remarkable difference is the change in the hydrogen bonding

length from the ground to the excited state. For E_{cis} in the S_1 , CAM-B3LYP gave a longer bond length than PBE1PBE and the opposite was observed for the keto tautomer.

The vertical excitation energies and oscillator strengths calculated for structures **3a** and **3b** are presented in Tables 5 and 6, respectively. TD-DFT vertical excitation energies were in good agreement with experimental ones. Consistent with previous works,⁸⁰⁻⁸¹ PBE1PBE energies were lower than experimental values, while CAM-B3LYP energies were higher than the experimental ones. On the other hand, the results provided by both functionals for the vertical emission energies were substantially different, mainly for the keto tautomers.

Another remarkable difference was that, while CAM-B3LYP provided excitation energies for enol and keto tautomers close to each other, this difference was much larger (around 200 nm) when PBE1PBE was used. For **3a**, CAM-B3LYP gave results closer to the experimental ones. However, comparing the experimental emission energies with the calculated ones, it is not easy to identify which functional provides a better result. The experimental data show higher emission energies for **3b** compared to **3a**. However, the energy differences between keto and enol conformers in the S_1 state (ΔE^*), show that ESIPT is more disfavoured for compound **3b** than for **3a**. Negative values indicated that the keto tautomer is more stable than the enol tautomer. From these values, there is an apparent different trend when using PBE1PBE and CAM-B3LYP functionals. Using the first one, the **3a** keto form is most stable

in low polarity solvents, and the two tautomeric forms are almost degenerated in ethanol and acetonitrile. On the other hand, the CAM-B3LYP functional suggests that the enol form is more stable in all the solvents. For **3b**, only in 1,4-dioxane (using PBE1PBE) the keto form is the most stable. Yet, the energy differences between the keto and enol forms are larger in **3b** than in **3a**. A common characteristic for these molecules using both functionals is that solvents with higher dielectric constant should disfavour the ESIPT mechanism, a finding in agreement with previous work.⁸² It is worth mentioning that compounds **3a** and **3b** presents in 1,4-dioxane and acetonitrile similar excitations and transition orbitals (see ESI). Due to the significant difference between CAM-B3LYP and PBE1PBE results, we decided to benchmark the TD-DFT functionals for these molecules. The vertical energies were compared to those obtained using RI-CC2 (Table 7). These calculations were done in the gas phase by using the geometries obtained with PBE1PBE and CAM-B3LYP. RI-CC2 offers a computationally efficient route to recover electron correlation and has been used as a reference value for ESIPT calculations.^{21,48,78} Comparing the TD-DFT excitation energies, it was observed that, in general, CAM-B3LYP provided results in better agreement with RI-CC2 calculations. This fact seems to indicate an ICT character for the S_1 state since it is well known that ICT states are better described using long-range corrected functionals.

Table 5 Absorption maxima (λ_{abs}) and emission wavelengths (λ_{em}), in nm, respective of oscillator forces (f), and energy differences between the keto and enol forms (ΔE^* , in eV), in the corresponding solvents, calculated for **3a**. The energies were calculated using the jun-cc-pVTZ basis set.

SOLVENT	PBE1PBE					CAM-B3LYP					
	λ_{abs} (nm)	f	λ_{em} (nm)	f	ΔE^* (eV)	λ_{abs} (nm)	f	λ_{em} (nm)	f	ΔE^* (eV)	
E_{cis}	1,4-Dioxane	404	0.688	465	0.559	-	342	1.038	391	1.172	-
	Dichloromethane	422	0.633	507	0.715	-	349	0.994	427	1.341	-
	Ethanol	426	0.602	520	0.757	-	351	0.960	439	1.383	-
	Acetonitrile	426	0.595	523	0.765	-	351	0.951	441	1.390	-
K_{cis}	1,4-Dioxane	475	0.299	678	0.103	-0.20	381	0.764	430	0.612	0.12
	Dichloromethane	478	0.315	647	0.217	-0.03	379	0.776	441	0.898	0.20
	Ethanol	477	0.309	641	0.262	0.01	378	0.758	446	0.966	0.21
	Acetonitrile	477	0.306	641	0.271	0.02	377	0.752	447	0.978	0.21

* $\Delta E = E_{keto} - E_{enol}$; 1 eV = 23.0609 kcal·mol⁻¹

Table 6 Absorption maxima (λ_{abs}) and emission wavelengths (λ_{em}), in nm, respective of oscillator forces (f) and energy differences between the keto and enol forms (ΔE^* , in eV), in the corresponding solvents, calculated for **3b**. The energies were calculated using the jun-cc-pVTZ basis set.

SOLVENT	PBE1PBE					CAM-B3LYP					
	λ_{abs} (nm)	f	λ_{em} (nm)	f	ΔE^* (eV)	λ_{abs} (nm)	f	λ_{em} (nm)	f	ΔE^* (eV)	
E_{cis}	1,4-Dioxane	403	0.754	459	0.591	-	342	1.117	387	1.263	-
	Dichloromethane	420	0.711	496	0.777	-	350	1.095	422	1.448	-
	Ethanol	423	0.682	508	0.827	-	351	1.067	433	1.494	-
	Acetonitrile	424	0.676	510	0.837	-	351	1.060	435	1.502	-
K_{cis}	1,4-Dioxane	454	0.288	677	0.059	-0.04	371	0.781	429	0.497	0.30
	Dichloromethane	455	0.329	636	0.144	0.15	371	0.840	430	0.857	0.41
	Ethanol	454	0.329	626	0.196	0.19	370	0.835	432	0.59	0.42
	Acetonitrile	454	0.328	625	0.207	0.20	369	0.832	433	0.977	0.43

* $\Delta E = E_{keto} - E_{enol}$; 1 eV = 23.0609 kcal·mol⁻¹

Table 7 Energy differences (in eV) between the ground state enol-cis and keto-cis (ΔE_{k-c}) and enol-cis and keto-trans (ΔE_{tk-c}), vertical absorption energies at ground state geometry ($\Delta E_{vert}(S_0^0)$) and vertical emission energies

from enol- S_1 ($\Delta E_{\text{vert}}(S_1^e)$) and from keto- S_1 ($\Delta E_{\text{vert}}(S_1^k)$). The energies were calculated in the gas phase.

	RICC2	CAMB3LYP	PBE1PBE	Exp. ^c	
3a	$\Delta E_{\text{k-E}}(S_1)$		0.13*	-0.20*	-
	$\Delta E_{\text{tk-E}}(S_1)$		0.21*	-0.16*	-
	$\Delta E_{\text{vert}}(S_0^e)$	3.70 ^a	3.81	3.29	
		3.70 ^b	3.63*	3.07*	3.28*
	$\Delta E_{\text{vert}}(S_1^e)$	3.39 ^a	3.45	2.85	
		3.49 ^b	3.17*	2.66*	2.49*
	$\Delta E_{\text{vert}}(S_1^k)$	2.73 ^a	2.86	1.74	
		2.56 ^b	2.88*	1.83*	2.49*
3b	$\Delta E_{\text{k-E}}$		0.30	-0.04	-
	$\Delta E_{\text{tk-E}}$		0.29	0.07	-
	$\Delta E_{\text{vert}}(S_0^e)$	3.69 ^a	3.81	3.30	
		3.69 ^b	3.62*	3.07*	3.21*
	$\Delta E_{\text{vert}}(S_1^e)$	3.45 ^a	3.48	2.87	
		3.55 ^b	3.21*	2.70*	2.45*
	$\Delta E_{\text{vert}}(S_1^k)$	2.69 ^a	2.85	1.72	
		2.57 ^b	2.89*	1.83*	2.45*

*Calculated in 1,4-dioxane; ^ageometry obtained with CAM-B3LYP/cc-pVDZ; ^bgeometry obtained with PBE1PBE/cc-pVDZ and ^cexperiment performed in 1,4-dioxane.

To further analyse the possibility of ESIPT in **3a** and **3b**, the potential energy curves for the proton-transfer in the S_1 state were also computed compared to the curves obtained for HBO, a well-known example of ESIPT (Fig. 7). These curves were computed by keeping the O–H bond distance in a range of values that increased in steps of 0.05 Å and optimising the remaining coordinates without constraints. CAM-B3LYP and PBE1PBE provided different barriers for the proton transfer, as well as present inversion on the relative stability between both tautomers. The calculated barriers for HBO are in agreement with the ones calculated by Roohi *et al.* using PBE1PBE/6-311++G(2d,p)^{76,83} and Alarcos *et al.*²³ using CAM-B3LYP/6-31G(d,p).

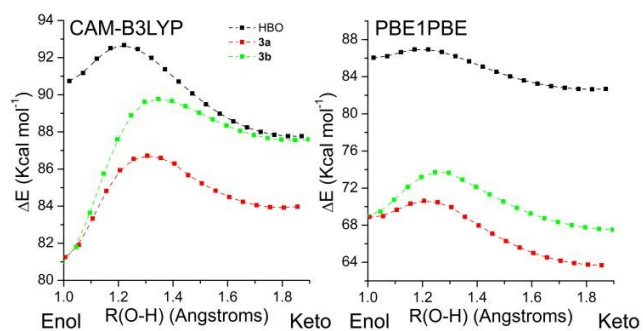


Fig. 7 Potential energy curves in the first excited state, with different O–H bond lengths, for HBO, **3a** and **3b** computed with TD-DFT.

Using CAM-B3LYP, for HBO the keto tautomer is clearly more stable (~ 3 kcal·mol⁻¹) and there the barrier for the ESIPT is very small (less than 2 kcal·mol⁻¹). Using PBE1PBE both, the energy difference between the two tautomers and the energy barrier, decreased. In contrast, CAM-B3LYP calculations for **3a** and **3b** show that the enol tautomer was the most stable. Yet, the energy barriers for the proton transfer are equal to 5.5 and

8.8 kcal·mol⁻¹, respectively. Moreover, PBE1PBE calculations indicated barriers of 1.7 and 4.6 kcal·mol⁻¹ for **3a** and **3b**, respectively. These results are an additional indication that ESIPT is disfavoured in the studied molecules, when compared to HBO. The specific substituent groups give a push-pull character for the molecules, which increases the possibility of ICT. Since the inclusion of these substituents affects the charge distribution of the proton donor and acceptor, it is interesting to evaluate not only the orbitals involved in the transition but also the electronic density over the atoms.

Regarding the solvent effect, the calculations showed a small influence of solvent polarity on absorption energies, a finding in agreement with the experimental results. A more significant effect was observed for the emission energies, where a redshift can be seen for the enol and keto forms using the CAM-B3LYP functional. In this case, the solvent polarity effect was larger for the enol than to the keto tautomer. This implies that S_1 for the enol is more polar than S_1 for the keto form (see Table 8). Therefore, polar environments stabilise the enol tautomer more than the keto tautomer, and shift the emission spectra to higher wavelengths. For this reason, the energy difference between the tautomers in the S_1 state is larger in more polar solvents, and emission from the keto tautomer should be more disfavoured. Consequently, is expected that the fluorescence spectra shows a double emission in non-polar solvents, where keto tautomers are more easily reached. Interestingly, PBE1PBE showed a different trend (blueshift) for the keto form with the increase of the solvent polarity.

Fig. 8 shows the molecular orbitals involved in the transitions from the ground to the first excited state. The first excitation is predominantly from the highest occupied molecular orbital (HOMO) to the lowest unoccupied molecular orbital (LUMO) and it has a $\pi\pi^*$ character.

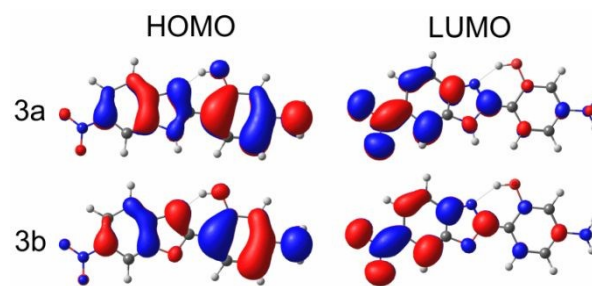
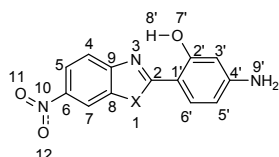


Fig. 8 Molecular orbitals calculated for **3a** and **3b** using CAM-B3LYP.

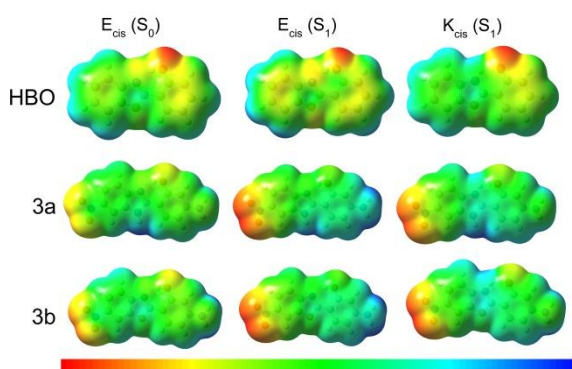
It can be noticed that the heteroatom in the benzazole unit has a negligible effect. For **3a** and **3b**, HOMO is delocalised over almost the entire molecule, excluding the nitro group. Significant electron density is located over the nitrogen of the amino group and over the hydroxyl group. The LUMO is mainly delocalised over the fused rings and nitro group. This indicates that excitation to the S_1 state should transfer electron density from the side that contains the amino group, the donor, to the

ARTICLE

Table 8 Partial ChelpG charges (in a.u.) and dipole momenta (μ , in D) calculated using 1,4-dioxane as solvent for HBO, **3a** (X=NH) and **3b** (X=O) using CAM-B3LYP and PBE1PBE (in italic) and the jun-cc-pVDZ basis set.


Structure	μ	N_3	$O_{7'}$	$H_{8'}$	X_1	$N_{9'}$	N_{10}	O_{11}	O_{12}
HBO (S_0)	2.6	-0.508	-0.567	0.345	-0.290				
	2.5	<i>-0.479</i>	<i>-0.536</i>	<i>0.337</i>	<i>-0.264</i>				
HBO (S_1 -E)	1.6	-0.545	-0.528	0.373	-0.303				
	1.4	<i>-0.526</i>	<i>-0.499</i>	<i>0.373</i>	<i>-0.276</i>				
HBO (S_1 -K)	3.7	-0.466	-0.655	0.420	-0.275				
	2.7	<i>-0.459</i>	<i>-0.630</i>	<i>0.427</i>	<i>-0.253</i>				
3a (S_0)	8.6	-0.562	-0.592	0.365	-0.598	-0.794	0.739	-0.457	-0.472
	9.2	<i>-0.533</i>	<i>-0.558</i>	<i>0.355</i>	<i>-0.574</i>	<i>-0.752</i>	<i>0.703</i>	<i>-0.444</i>	<i>-0.457</i>
3a (S_1 -E)	20.8	-0.528	-0.551	0.368	-0.583	-0.898	0.661	-0.565	-0.570
	28.0	<i>-0.484</i>	<i>-0.509</i>	<i>0.357</i>	<i>-0.544</i>	<i>-0.805</i>	<i>0.597</i>	<i>-0.580</i>	<i>-0.596</i>
3a (S_1 -K)	16.3	-0.467	-0.638	0.434	-0.504	-0.769	0.672	-0.557	-0.557
	24.4	<i>-0.473</i>	<i>-0.581</i>	<i>0.440</i>	<i>-0.522</i>	<i>-0.761</i>	<i>0.585</i>	<i>-0.584</i>	<i>-0.598</i>
3b (S_0)	7.8	-0.533	-0.569	0.352	-0.287	-0.798	0.740	-0.454	-0.463
	8.5	<i>-0.503</i>	<i>-0.537</i>	<i>0.342</i>	<i>-0.254</i>	<i>-0.760</i>	<i>0.705</i>	<i>-0.440</i>	<i>-0.449</i>
3b (S_1 -E)	19.6	-0.489	-0.539	0.358	-0.300	-0.899	0.690	-0.556	-0.558
	27.8	<i>-0.442</i>	<i>-0.487</i>	<i>0.340</i>	<i>-0.265</i>	<i>-0.789</i>	<i>0.617</i>	<i>-0.579</i>	<i>-0.589</i>
3b (S_1 -K)	12.7	-0.491	-0.637	0.447	-0.262	-0.779	0.699	-0.519	-0.519
	25.5	<i>-0.510</i>	<i>-0.577</i>	<i>0.454</i>	<i>-0.239</i>	<i>-0.903</i>	<i>0.594</i>	<i>-0.581</i>	<i>-0.591</i>

side containing the nitro group, the acceptor. The spatial separation of HOMO and LUMO orbitals is characteristic of push-pull molecules and indicates a charge transfer from one side to the other (see Fig. 9). These results are consistent with the charge distribution and with the fact that ICT should overarch ESIPT in both **3a** and **3b**.

**Fig. 9** Electrostatic potential surfaces for HBO, **3a** and **3b** obtained using CAM-B3LYP.

Phototautomerism is associated with changes in electronic densities and to a certain amount of charge transferred between the acceptor and donor atoms. Further, charge transfer states are characterised by changes in the electronic density from one side of the molecule to the other. Therefore, it is interesting to analyse the redistribution of electronic charges after the excitation. Table 8 shows the charge distribution and dipole moment for HBO, **3a** and **3b** in S_0 -enol, S_1 -enol and S_1 -keto. From S_0 - to S_1 -enol, the negative charge over $O_{7'}$ decreased for all three molecules, but for HBO the proton $H_{8'}$ became much more positive than for **3a** and **3b**, highlighting the increase in the proton donor acidity mainly for the former molecule. Additionally, the electronic density over the N_3 atom in HBO increase and enhance its basicity, as expected.⁸⁴ As a result, a fast proton transfer takes place from the donor to the acceptor atom along the reaction coordinate in the S_1 . On the other hand, for **3a** and **3b**, the electronic density on the N_3 atom decreases after excitation and relaxation to the enol form, indicating a decrease in the basicity of the

acceptor atom and, therefore, disfavoring the ESIPT. This fact can indicate that the electronic density is shifted to other atoms in **3a** and **3b**. Indeed, going from the S_0 - to S_1 -enol, there was a large increase (~ 0.1 a.u.) in the negative charge over O_{11} and O_{12} , a change that emphasizes the increase of electronic density shifted by the ICT process.

The changes in electronic density can be easily observed in the electrostatic potential surfaces plotted in Fig. 9. In HBO, the electronic density is mainly localised on the donor group and slightly spreads out over the benzene rings after excitation. However, after excitation in **3a** and **3b**, the electronic density is clearly shifted from the $-NH_2$ to the $-NO_2$ side, strongly indicating that ICT takes place. The changes in the electronic density are also reflected in the dipole momentum (μ) of the molecules and they can help to assign the character of the transitions. In HBO, μ undergoes a small variation in the excited state, indicating a LE character, in contrast to **3a** and **3b**. There is a large increase in the dipole moment when transitioning from S_0 to S_1 (particularly large for the enol tautomer), which is one more indicator of charge transfer states. The large increase in the dipole moment implies that polar solvents can stabilise ICT states more than nonpolar solvents by decreasing the energy gap between S_1 and S_0 .⁵⁸ Consequently, there is a redshift in the wavelengths in the emission spectra. This observation agrees with the calculated emission wavelengths presented in Tables 5 and 6.

It is worth noting that the PBE1PBE functional provided the wrong trend for keto emission, where λ_{em} decreased with increasing solvent polarity. This observation highlights the fact that the PBE1PBE functional does not describe charge transfer states properly. Our results agree with Hsieh *et al.*,³⁰ that show that when a large charge separation in the molecule is present, ICT should occur prior to ESIPT. In this case, with the increase of the solvent polarity, the emission wavelength should present a bathochromic effect. Additionally, solvent polarisation effects can be more easily observed since there is a significant difference in the dipole moment between both conformers in the excited state.³⁰

While most of the emission energies calculated for **3a** using CAM-B3LYP were fully in agreement with experimental results, this concurrence was not observed for 1,4-dioxane. A possible explanation can be rationalised in terms of the energy profiles given in Fig. 10. Although the enol form is the most stable one, the energy difference between the two tautomers is very small (0.12 eV). In addition, the energy barrier for the proton transfer is equal to the relaxation energy for the Franck-Condon state. Therefore, after the light absorption, the system still has enough energy to overcome the barrier and populate the keto form to some extent. This fact implies that the abnormally larger wavelength observed experimentally for **3a** in 1,4-dioxane could be associated with the emission from keto tautomer. This supposition supports the mechanism of ICT coupled to ESIPT for **3a** in 1,4-dioxane, while the emission in the remaining solvents is attributed to an ICT.

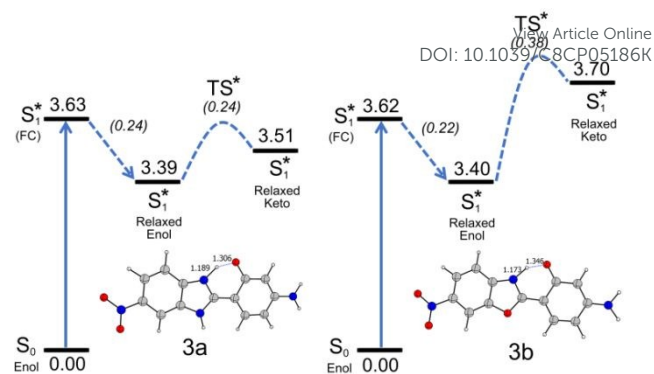


Fig. 10 Energy profiles in the first excited state for **3a** (left) and **3b** (right) in 1,4-dioxane calculated using CAM-B3LYP/jun-cc-pVDZ. The inserts show the geometries that correspond to the transition states and the N-H and O-H distances (in Å). Energies were calculated in relation to the S_0 -enol optimized structure, except the values in parenthesis, which represent the energy difference between the states connected by the dashed line and the transition state energy.

The situation is different for **3b**. For this compound, the vertical absorption does not provide enough energy to the molecules to overcome the barrier for the proton transfer since the keto tautomer has even higher energy than FC transition. Therefore, the higher wavelengths experimentally observed for **3b** when compared to **3a** were not reproduced in the calculations and the reason for this discrepancy remains unclear. Additionally, according to calculations, changing the heteroatom from N to O does not impact considerably the emission energy, in contrast to the experimental results. A possible explanation for both effects could be associated to specific interactions with the solvent molecules. Our current research will explore these directions.

Additional calculations using explicit solvent (molecules of acetonitrile plus implicit solvation) clearly show the effect of this solvent in the emission spectra (for the plots of spectra and molecular orbitals see supporting information). While the LE band (around 300 nm) remains basically unchanged with the addition of acetonitrile molecules, the ICT band is clearly redshifted (from ~ 440 nm to ~ 470 nm). This is a strong evidence for ICT.

Conclusions

The synthesised compounds **3a** and **3b** presented in solution absorption maxima in the UVA-visible region due to spin and symmetry allowed electronic $1\pi\pi^*$ with no clear evidence for charge transfer in either compound in the ground state. In general, two states, LE and ICT could be observed for compounds **3a** and **3b**, which were tailored by solvent polarity, leading to fluorescence emission in the violet-blue-green region. Taking the longer-wavelength emission in the into account, experimentally this work has also established that: (a) relatively large Stokes shifts were observed for **3a** and **3b**, (b) compound **3b** was more polar in the excited state than **3a**, (c) excited state deactivation seemed to be ascribed to ICT, observed from the Lippert-Mataga correlation in the Δf range of 0.02-0.20 and (d) at higher Δf the medium polarity seems to

reach a limit of stabilisation. In summary, experimentally, charge-transfer emissions seems to be responsible prior to ESIPT, to the long-emission wavelengths in these compounds. To further investigate the possibility of ESIPT or ICT, we performed TD-DFT calculations. They also indicate that ICT should take place prior to ESIPT. ESIPT is largely disfavoured mainly in polar solvents. The emission wavelengths were sensitive to the solvent polarity, in agreement with the occurrence of ICT. For **3a** in 1,4-dioxane, the small energy difference between the tautomeric forms added to the small energy barriers, allow the emission from the keto.

Acknowledgements

The authors would like to thank FAPERGS (17/2551-0000968-1), CNPq and Coordenação de Aperfeiçoamento de Pessoal de Nível Superior - Brasil (CAPES) - Finance Code 001 for the financial support. Theoretical calculations were carried out with the support of Centro Nacional de Supercomputação (CESUP), from the Universidade Federal do Rio Grande do Sul and National Laboratory of Scientific Computation (LNCC-Santos Dumond).

Notes and references

- 1 A. Z. Weller, *Electrochem.*, 1956, **42**, 1144.
- 2 H. K. Sinha and S. K. Dogra, *Chem. Phys.*, 1986, **12**, 337.
- 3 A. P. Demchenko, K. C. Tang and P. T. Chou, *Chem. Soc. Rev.*, 2013, **42**, 1379.
- 4 J. E. Kwon and S. Y. Park, *Adv. Mater.*, 2011, **23**, 3625.
- 5 F. S. Santos, E. Ramasamy, V. Ramamurthy and F. S. Rodembusch, *J. Photochem. Photobiol. A Chem.*, 2016, **317**, 175.
- 6 F. S. Santos, N. G. Medeiros, R. F. Affeldt, R. D. Duarte, S. Moura and F. S. Rodembusch, *New J. Chem.*, 2016, **40**, 2785.
- 7 R. Wang, D. Liu, K. Xu and J. Li, *J. Photochem. Photobiol. A Chem.*, 2009, **205**, 61.
- 8 P. O. Hubin, A. D. Laurent, D. P. Vercauteren and D. Jacquemin, *Phys. Chem. Chem. Phys.*, 2014, **16**, 25288.
- 9 N. Jiang, C. Yang, X. Dong, X. Sun, D. Zhang and C. Liu, *Org. Biomol. Chem.*, 2014, **12**, 5250.
- 10 J. Zhao, S. Ji, Y. Chen, H. Guo and P. Yang, *Phys. Chem. Chem. Phys.*, 2012, **14**, 8803.
- 11 V. A. Corbellini, M. L. Scroferneker, M. Carissimi, F. S. Rodembusch and V. Stefani, *J. Photochem. Photobiol. B Biol.*, 2010, **99**, 162.
- 12 K. Dhanunjayarao, V. Mukundam and K. Venkatasubbaiah, *Sens. Actuators B*, 2016, **232**, 175.
- 13 H. M. Lv, D. H. Yuan, W. Liu, Y. Chen, C. T. Au and S. F. Yin, *Sens. Actuators B*, 2016, **233**, 173.
- 14 A. Maity, F. Ali, H. Agarwalla, B. Anothumakkool and A. Das, *Chem. Commun.*, 2015, **51**, 2130.
- 15 U. N. Yadav, H. S. Kumbhar, S. S. Deshpande, S. K. Sahoob and G. S. Shankarling, *RSC Adv.*, 2015, **5**, 42971.
- 16 M. Luo, S. Wang, M. Wang, S. Huang, C. Li, L. Che and X. Ma, *Dyes Pigm.*, 2016, **132**, 48.
- 17 Turro, N. J. In. *Modern Molecular Photochemistry*; University Science Books: Sausalito, 1991; pp. 628.
- 18 A. J. A. Aquino, F. Plasser, M. Barbatti and H. Lischka, *Croat. Chem. Acta*, 2009, **1**, 105. DOI: 10.1039/C8CP05186K
- 19 O. K. Abou-Zied, R. Jimenez, E. H. Thompson, D. P. Millar and F. E. Romesberg, *J. Phys. Chem. A*, 2002, **106**, 3665.
- 20 W. Frey and T. Elsaesser, *Chem. Phys. Lett.*, 1992, **189**, 565.
- 21 M. Barbatti, A. J. A. Aquino, H. Lischka, C. Schrieffer, S. Lochbrunner and E. Riedle, *Phys. Chem. Chem. Phys.*, 2009, **11**, 1406.
- 22 C. Schrieffer, M. Barbatti, K. Stock, A. J. A. Aquino, D. Tunega, S. Lochbrunner, E. Riedle, R. de Vivie-Riedle and H. Lischka, *Chem. Phys.*, 2008, **347**, 446.
- 23 N. Alarcos, M. Gutiérrez, M. Liras, F. Sánchez, M. Moreno and A. Douhal, *Phys. Chem. Chem. Phys.* 2015, **17**, 14569.
- 24 N. Alarcos, M. Gutierrez, M. Liras, F. Sánchez and A. Douhal, *Phys. Chem. Chem. Phys.*, 2015, **17**, 16257.
- 25 S. Pijeau, D. Foster and E.G. Hohenstein, *J. Phys. Chem. A* 2017, **121**, 4595.
- 26 T. C. Swinney and D. F. Kelley, *J. Chem. Phys.*, 1993, **99**, 211.
- 27 J. Seo, S. Kim and S. Y. Park, *J. Am. Chem. Soc.*, 2004, **126**, 11154.
- 28 V. I. Tomin, A. P. Demchenko and P. T. Chou, *J. Photochem. Photobiol. C Photochem. Rev.*, 2015, **22**, 1.
- 29 P. Chowdhury, S. Panja, A. Chatterjee, P. Bhattacharya and S. Chakravorti, *J. Photochem. Photobiol. A Chem.*, 2005, **170**, 131.
- 30 C. C. Hsieh, Y. M. Cheng, C. J. Hsu, K. Y. Chen and P. T. Chou, *J. Phys. Chem. A*, 2008, **112**, 8323.
- 31 F. S. Rodembusch, F. P. Leusin, L. F. Campo and V. Stefani, *J. Lumin.*, 2007, **126**, 728.
- 32 S. Hillebrand, M. Segala, T. Backup, R. R. B. Correia, F. Horowitz and V. Stefani, *Chem. Phys.*, 2001, **273**, 1.
- 33 J. Seo, S. Kim, S. Park and S. Y. Park, *Bull. Korean Chem. Soc.*, 2005, **26**, 1706.
- 34 C. Li, Y. Yang, C. Ma and Y. Liu, *RSC Adv.*, 2016, **6**, 5134.
- 35 C. H. Kim, P. Jaehun, J. Seo, S. Y. Park and T. Joo, *J. Phys. Chem. A*, 2010, **114**, 5618.
- 36 M. Gutierrez, N. Alarcos, M. Liras, F. Sanchez and A. Douhal, *J. Phys. Chem. B*, 2015, **119**, 552.
- 37 C. Li, C. Ma, D. Li and Y. Liu, *J. Lumin.*, 2016, **172**, 29.
- 38 N. Alarcos, M. Gutierrez, M. Liras, F. Sanchez and A. Douhal, *Photochem. Photobiol. Sci.*, 2015, **14**, 1306.
- 39 J. P. Perdew, K. Burke and M. Ernzerhof, *Phys. Rev. Lett.*, 1996, **77**, 3865.
- 40 T. Yanai, D. P. Tew and N. C. Handy, *Chem. Phys. Lett.*, 2004, **393**, 51.
- 41 W. L. F. Armarego. In *Purification of Laboratory Chemicals*, 5th ed.; Cornwall, UK: Elsevier Academic Press; 2003.
- 42 A. Chekalyuk, V. Fadeev, G. Georgiev, T. Kalkanjiev and Z. Nickolov, *Spectrosc. Lett.*, 1982, **15**, 355.
- 43 F. S. Rodembusch, T. Backup, M. Segala, L. Tavares, R. R. B. Correia and V. Stefani, *Chem. Phys.*, 2004, **305**, 115.
- 44 S. Hammes-Schiffer and A. A. Stuchebrukhov, *Chem. Rev.*, 2010, **110**, 6939.
- 45 S. Lubner, K. Adamczyk, E. T. J. Nibbering and V. S. Batista, *J. Phys. Chem. A*, 2013, **117**, 5269.
- 46 R. S. Iglesias, L. F. Campo, F. S. Rodembusch and V. Stefani, *Int. J. Quantum Chem.*, 2004, **108**, 2334.
- 47 A. J. A. Aquino, H. Lischka and C. Hättig, *J. Phys. Chem.*, 2005, **109**, 3201.
- 48 N. Kungwan, F. Plasser, A. J. A. Aquino, M. Barbatti, P. Wolschmann and H. Lischka, *Phys. Chem. Chem. Phys.*, 2012, **14**, 9016.

- 49 L. Wang, Y. Zhang, Y. Li, H. He and J. Zhang, *J. Photochem. Photobiol. A Chem.*, 2014, **294**, 14.
- 50 W. Yang and X. Chen, *Phys. Chem. Chem. Phys.*, 2014, **16**, 4242.
- 51 J. M. Ortiz-Sánchez, R. Gelabert, M. Moreno and J. M. Lluch, *J. Chem. Phys.*, 2008, **129**, 214308.
- 52 A. Fernández-Ramos, E. Martínez-Núñez, S. A. Vázquez, M. A. Ríos, C. M. Estévez, M. Merchán and L. Serrano-Andrés, *J. Phys. Chem. A*, 2007, **111**, 5907.
- 53 Plasser, F. In: Dynamics simulation of excited state intramolecular proton transfer; Master Thesis, Zentrum für Molekulare Biologie, Universität Wien: Viena, 2009.
- 54 E. Papajak, J. Zheng, H. R. Leverentz and D. G. Truhlar, *J. Chem. Theory Comput.*, 2011, **7**, 3027.
- 55 M. Barbatti, A. J. A. Aquino, H. Lischka, C. Schriver, S. Lochbrunner and E. Riedle, *Phys. Chem. Chem. Phys.*, 2009, **11**, 1406.
- 56 A. Köhn and C. Hättig, *J. Chem. Phys.*, 2003, **119**, 5021.
- 57 TURBOMOLE V7.0 2015, a development of University of Karlsruhe and Forschungszentrum Karlsruhe GmbH, 1989–2007, TURBOMOLE GmbH, since 2007; available from <http://www.turbomole.com>.
- 58 J. R. Lakowicz, In: Principles of Fluorescence Spectroscopy, Springer, New York, 3rd edn, 2006, ch. 6, pp. 205–235.
- 59 P. S. Kalsi, In: *Spectroscopy of Organic Compounds*. New Age International Pvt Ltd Publishers; 6th edn., 2016.
- 60 S. J. Strickler and R. A. Berg, *J. Phys. Chem.*, 1962, **37**, 814.
- 61 N. J. Turro, J. C. Scaiano and V. Ramamurthy, In: *Principles of Molecular Photochemistry: An Introduction*. University Science Books; 1st edn., 2008.
- 62 G. Calzaferri and R. Rytz, *J. Phys. Chem.*, 1995, **9**, 12141.
- 63 S. M. Ormson, R. G. Brown, F. Vollmer and W. Rettig, *J. Photochem. Photobiol. A Chem.*, 1994, **81**, 65.
- 64 S. A. El-Daly, A. M. Asiri and K. A. Alamry, *J. Fluoresc.*, 2014, **24**, 1307.
- 65 E. Lippert, W. Lüder, F. Moll, W. Nägele, H. Boos, H. Prigge and I. Seibold-Blankenstein, *Angew. Chem.*, 1961, **73**, 695.
- 66 S. R. Marder, G. D. Stucky and J. E. Sohn (Editors). In: *Materials for Nonlinear Optics. Chapter 1. Linear and Nonlinear Polarizability*. Publisher: American Chemical Society, Vol. 455, pp2-30, 1991.
- 67 M. S. Paley, J. M. Harris, H. Looser, J. C. Baumert, G. C. Bjorklund, D. Jundt and R. Twieg, *J. Org. Chem.*, 1989, **54**, 3774.
- 68 H. C. Song, Y. W. Chen, X. L. Zheng and B. N. Ying, *Spectrochim. Acta A*, 2001, **57**, 1717.
- 69 F. Momicchioli, G. Ponterini and D. Vanossi, *J. Phys. Chem. A*, 2008, **112**, 11861.
- 70 C. Reichardt, *Solvent Effects in Organic Chemistry*, Verlag Chemie: Weinheim, 1979.
- 71 A. Kowski, *Z. Naturforsch A* 2002, **57**, 255.
- 72 S. K. Lanke and N. Sekar, *J. Photochem. Photobiol. A Chem.*, 2016, **321**, 63.
- 73 E. G. McRae, *J. Phys. Chem.*, 1957, **61**, 562.
- 74 S. Bruni, E. Cariati, F. Cariati, F. Porta, S. Quici and D. Roberto, *Spectrochim. Acta A*, 2001, **57**, 1417.
- 75 <http://gaussian.com/volume/>, accessed in July 23, 2018
- 76 H. Roohi, N. Mohtamedifar and F. Hejazi, *Chem. Phys.* 2014, **444**, 66.
- 77 L. Wilbraham, M. Savarese, N. Rega, C. Adamo and I. Ciofini, *J. Phys. Chem. B*, 2015, **119**, 2459
- 78 O. Louant, B. Champagne and V. Liégeois, *J. Phys. Chem. A*, 2018, **22**, 972. DOI: 10.1039/C8CP05186K
- 79 R. S. Iglesias, P. F. B. Gonçalves and P. R. Livotto, *Chem. Phys. Lett.*, 2000, **327**, 23.
- 80 A. Laurent, D. Jacquemin, *Int. J. Quantum Chem.*, 2013, **113**, 2019.
- 81 C. Adamo and D. Jacquemin, *Chem. Soc. Rev.*, 2013, **42**, 845.
- 82 J. Hao and Y. Yang, *Org. Chem. Front.* **2018**, **5**, 2234.
- 83 H. Roohi, F. Hejazi, N. Mohtamedifar and M. Jahantab, *Spectrochim. Acta Part A*, 2014, **118**, 228.
- 84 C. Li, Y. Yang, C. Ma and Y. Liu, *RSC Adv.*, 2016, **6**, 5134.